Application of airborne photogrammetry for the visualisation and assessment of contamination migration arising from a Fukushima waste storage facility

AUTHOR(S):

Connor, D.T.; Martin, P.G.; Smith, N.T.; Payne, L.; Hutton, C.; Payton, O.D.; Yamashiki, Y.; Scott, T.B.

CITATION:

Connor, D.T. ...[et al]. Application of airborne photogrammetry for the visualisation and assessment of contamination migration arising from a Fukushima waste storage facility. Environmental Pollution 2018, 234: 610-619

ISSUE DATE:

2018-03

URL:

http://hdl.handle.net/2433/230439

Environmental Pollution 234 (2018) 610–619

Contents lists available at ScienceDirect

Environmental Pollution

journal homepage: www.elsevier.com/locate/envpol

Application of airborne photogrammetry for the visualisation and assessment of contamination migration arising from a Fukushima waste storage facility☆

D.T. Connor [a, *], P.G. Martin [a], N.T. Smith [b, c, d], L. Payne [a], C. Hutton [a], O.D. Payton [a], Y. Yamashiki [e], T.B. Scott [a]

[a] Interface Analysis Centre, HH Wills Physics Laboratory, University of Bristol, Bristol BS8 1TL, UK
[b] National Nuclear Laboratory, Chadwick House, Warrington WA3 6AE, UK
[c] Schools of Mechanical, Aerospace and Civil Engineering, The University of Manchester, Manchester M13 9PL, UK
[d] Earth and Environmental Sciences, The University of Manchester, Manchester M13 9PL, UK
[e] Graduate School of Advanced Integrated Studies in Human Survivability, Kyoto University, Kyoto, Japan

ARTICLE INFO

Article history:
Received 2 June 2017
Received in revised form
18 October 2017
Accepted 19 October 2017
Available online 21 December 2017

Keywords:
Fukushima
Contamination
UAV
Photogrammetry
Radiation
Migration

ABSTRACT

Airborne systems such as lightweight and highly portable unmanned aerial vehicles (UAVs) are becoming increasingly widespread in both academia and industry - with an ever-increasing range of applications, including (but not limited to), air quality sampling, wildlife monitoring and land-use mapping.

In this work, high-resolution airborne photogrammetry obtained using a multi-rotor system operating at low survey altitudes, is combined with ground-based radiation mapping data acquired at an interim storage facility for wastes removed as part of the large-scale Fukushima clean-up program. The investigation aimed to assess the extent to which the remediation program at a specific site has contained the stored contaminants, as well as present a new methodology for rapidly surveying radiological sites globally. From the three-dimensional rendering of the site of interest, it was possible to not only generate a powerful graphic confirming the elevated radiological intensity existing at the location of the waste bags, but also to also illustrate the downslope movement of contamination due to species leakage from the large 1m^3 storage bags. The entire survey took less than 1 h to perform, and was subsequently post-processed using graphical information software to obtain the renderings. The conclusions within this study not only highlight the usefulness of incorporating three-dimensional renderings within radiation mapping protocols, but also conclude that current methods of monitoring these storage facilities in the long term could be improved through the integration of UAVs within the standard protocol.

1. Introduction

March 2017 marked the six-year anniversary of the Fukushima Daiichi Nuclear Power Plant (FDNPP) accident that occurred on Japan's eastern coast. Like the Chernobyl accident that occurred twenty-five years earlier, the events at Fukushima were similarly rated at Level 7 on the INES ranking system (IAEA, 2008) – representing a severe incident with far-reaching global ramifications. In these succeeding years, a considerable amount of financial expense has been devoted to the study of the various forms of radiological contamination that were released into the environment, but also (and the focus of this work) in the remediation of the large areas of Fukushima Prefecture that were radiologically contaminated by the event.

The principal radioisotopes of concern are the highly-volatile fission product isotopes of cesium, ^{134}Cs and ^{137}Cs, with half-lives of 2.0652 and 30.1 years respectively. Both of these species are strong gamma-ray emitters – formed as fragments from the fissioning of the uranium dioxide fuel used in each of the plant's six nuclear reactors. As a result of this and the earlier Chernobyl accident, a large number of studies have examined the behaviour of radiocesium within the environment. These studies have confirmed that fine-scale cesium particles have a strong affinity for sorption on to the frayed-edge sites of microscopic clay minerals (e.g.

☆ This paper has been recommended for acceptance by Dr. Hageman Kimberly Jill.
* Corresponding author.
E-mail address: dean.connor@bristol.ac.uk (D.T. Connor).

https://doi.org/10.1016/j.envpol.2017.10.098

kaolinite, montmorillonite and smectite) and fine-scale mica minerals, both of which are common in soils and comprise a significant component of Fukushima-specific soil matrices. Once physically sorbed onto the active-sites, it has been shown that they then remain strongly bonded - even under harsh chemical regimes that would not exist within the environment. It is therefore considered that the transportation of cesium does not occur as discrete isolated particles, but rather in response to the movement of the larger minerals that they are bonded to.

As part of the extensive remediation program that is occurring within the north-west trending plume affected region of Fukushima Prefecture, the uppermost 15 cm of sediment material is being removed from all contaminated land surfaces along with forest and all other organic material. Once removed, this material is placed into approximately 1 m^3 high-density plastic storage bags, before being transported to interim storage facilities ahead of its final (yet to be fully determined) disposal within a long-term storage facility. It has estimated that approximately 30 million tonnes of contaminated soils and wastes will be produced following this large-scale remediation (Japanese Ministry of the Environment, 2012), producing over 10 million bags of waste material. The total cost of this remediation has been estimated to range from JPY1.55–5.12 trillion (depending on eventual dose-reduction and decontamination scenario selected), with upper estimates placed at potentially exceed JPY16 trillion, if all contaminated forest areas were similarly remediated (Yasutaka and Naito, 2015).

Many of these small-scale temporary storage facilities exist, with numerous interim storage facilities (ISF) located across the entire Fukushima Prefecture. They consist of a secured fenced enclosure within which several hundred of the storage bags are carefully stacked - typically between four and eight units high (Fig. 1). Prior to the location of storage bags the storage facility must first be made suitable. This preparation includes the underlining of the entire site with an impermeable geo-polymer before being overlain by a thickness of imported made-ground (Fig. 1). After preparation of each of the facilities is completed, a vent network is installed in order to ensure flammable gases (produced as a result of anaerobic decomposition) do not build-up within the site. Finally, an impermeable cover is placed over the completed stack to severely limit water-ingress.

During facility preparation, the large black waste bags (stacked in an offset-cubic arrangement) are not protected against the effects of water ingress from the typhoon-type meteoric conditions typical of the region (Japan Meteorological Agency) – it is only after completion of preparation works that the site is made water-tight. As well as being classified climatically as typhoon-affected, the topography of the Fukushima Prefecture region also presents several challenges to the remediation effort. In addition to the inherent difficulties associated with the physical removal of material from the landscape, the mountainous terrain associated with the Abukuma Mountains (which constitute a considerable portion of the plume-affected region) represents a further issue with respect to the long-term environmental remediation of the region when combined with the heavy rainfall experienced. As has been concluded in several works (Nagao et al., 2013; Ueda et al., 2013; Yamaguchi et al., 2012) investigating the downslope movement of material (and hence radiation), the enhanced topography is responsible for dramatically increasing the rate at which this transport occurs.

Building from the conclusions and findings of earlier work developing UAV-based radiation mapping techniques (MacFarlane et al., 2014; Martin et al., 2015, 2016a, 2016b, 2016c; Connor et al., 2016), the following text outlines the methods employed to create a three-dimensional (3D) radiation map of an interim storage facility within the Fukushima Prefecture (Fig. 2). The site in question sits around 35 km north-west from the Fukushima Daiichi Nuclear Power Plant (FDNPP). Within this zone, a large number of bags containing contaminated topsoil have been placed for storage, with further bags still to be added at the time of the investigation (October 2016). The process of infilling the bags and placing them on-site takes approximately between 2 and 4 months to complete from initiation. During this time, the site in question experienced anywhere between 494 and 794 mm^3 precipitation (Japan Meteorological Agency), which could feasibly create a contaminant transport pathway downslope of the bale stack. The objective of the current work was to successfully constrain the relationship between the precipitation, topography and distribution of radiological material across the interim storage facility. Low-altitude aerial photogrammetry is employed to create a high resolution digital surface model (DSM), which is overlain with a colour-scaled

Fig. 1. Photograph of a typical waste storage study site within Kawamata (Date District), Fukushima Prefecture, prior to final waterproofing of the structure.

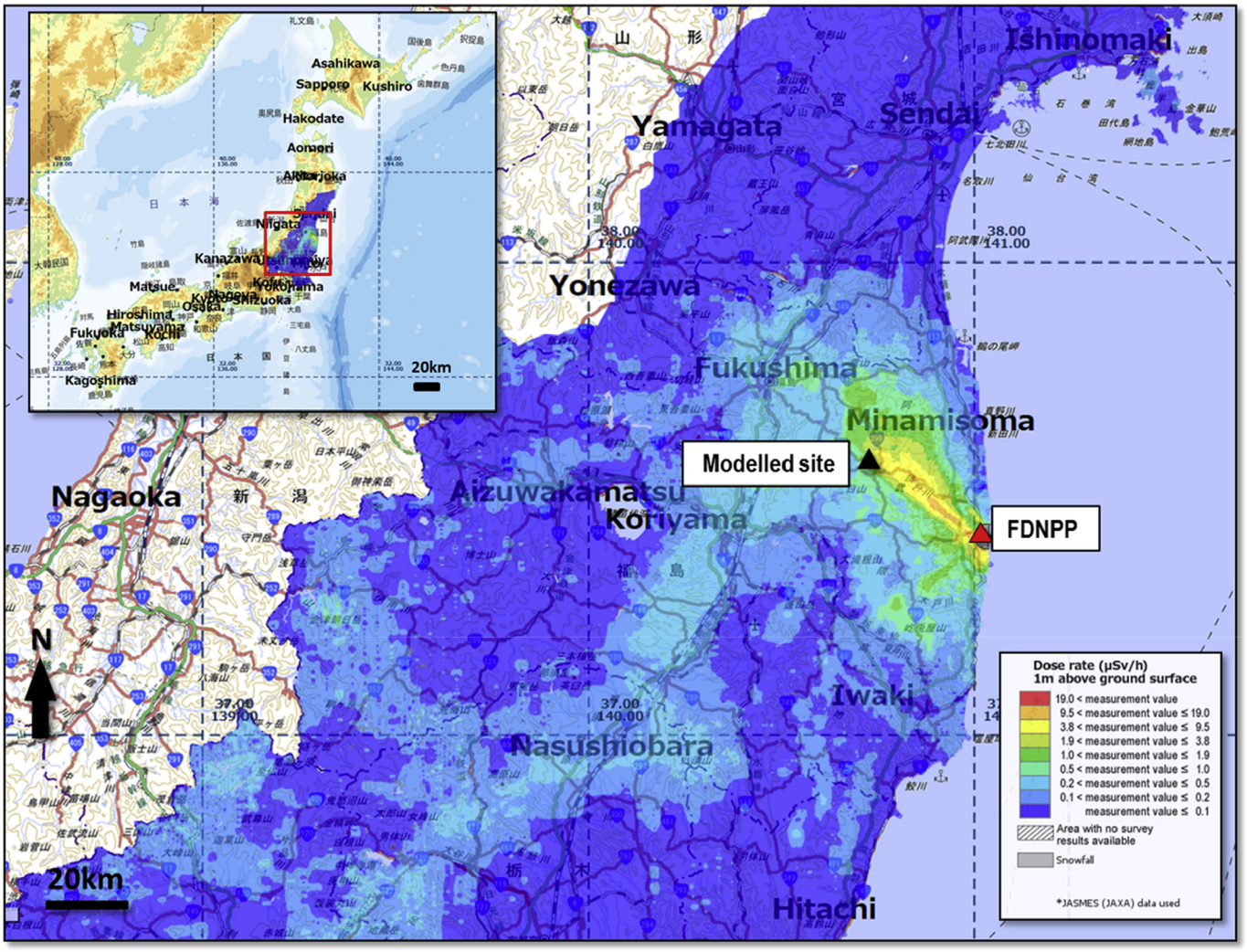

Fig. 2. A regional map view of the location of the modelled site and its proximity to the Fukushima Daiichi Nuclear Power Plant (FDNPP). Air dose rates were obtained from publicly available data supplied by the JAEA (JAEA, 2017).

radiation overlay processed from data obtained by a novel backpack-hosted dual detector system. The arising 3D radiation map is compared with hydrological simulations derived from the produced DSM to delineate the relationship between the surface water movement and distribution of radiological material across the site. Such a methodology would prove useful for the monitoring and implementation of site remediation works throughout the region.

2. Experimental

2.1. Radiation mapping

The basic platform used to conduct the radiation mapping of the site is described in earlier works by the authors (Martin et al., 2016a). However, as part of this work, an advancement to the system was made to enhance the rate of coverage, total sensitivity and spectral resolution. A schematic of the system is shown in Fig. 3 (a).

At present, the radiological monitoring work within the ISF sites and the wider Fukushima Prefecture is conducted through the use of single-spectrometer, ground-based radiation mapping systems. These surveys are often conducted by different operators for the same site at different times, meaning that comparability of the results produced from the survey are questionable. This new system comprises a 2.3 m length of low-density polypropylene piping, 80 mm in internal diameter, attached to the backpack of the operator. At either end of the tubing, at the two points furthest away from the operator, are located the two radiation detectors and their associated GPS receivers. The specific units used within this system are Adafruit™ Ultimate GPS receivers. These units are capable of recording position at a rate between 1 and 10 Hz and present an absolute position accuracy of sub-three metres (Adafruit). The separation of the two units was in total 2.3 m; with a distance of 1 m existing between each of the two detectors and the centrally-positioned operator. At their position away from the operator, the effects of bodily-attenuation that can reduce measurement values by approximately 35% (Buchanan et al., 2016; Jones and Cunningham, 1983) are eliminated/considerably reduced. The advantage of using this dual detector configuration over simply correcting the recorded data for the attenuation by the operator is that it removes the need for an operator specific correction in the calibration process. As no two operators will have exactly the same body masses/shapes, differing levels of attenuation will be occurring between different surveys of the same area. Whilst this not only makes the data simpler to process post-

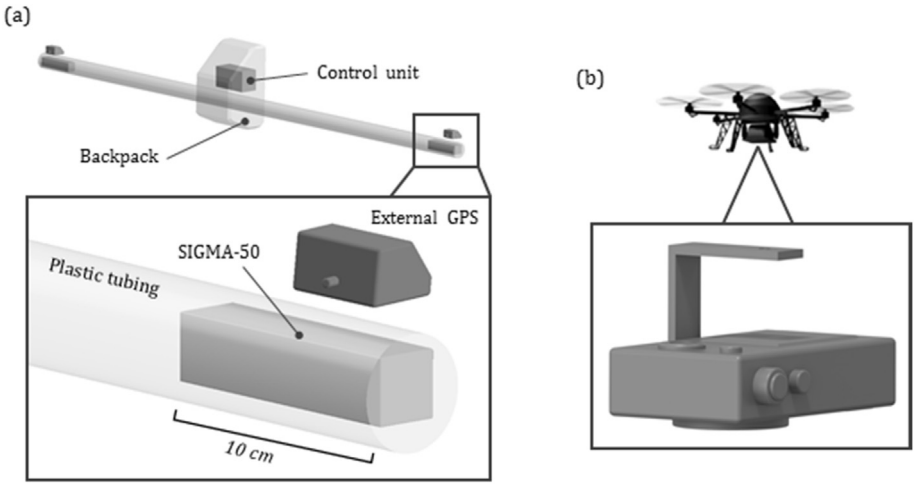

Fig. 3. Graphical representation and image of the (a) the two-detector ground-based radiation mapping system and (b) low-altitude unmanned aerial vehicle equipped with digital camera for photogrammetry reconstruction.

collection, it also means that the equipment can be used by different operators throughout time without losing repeatability/comparability between the results recorded in separate surveys in the same area.

For this work, two SIGMA-50™ (Kromek Ltd., Co. Durham, UK) NaI(Tl) gamma-ray spectrometers were used - over the smaller GR1™ (Kromek Ltd., Co. Durham, UK) cadmium zinc telluride (CZT) detectors employed previously. Each of these detectors consisted of a 1″ x 1″ x 2″ single crystal of scintillator material encased within a 1 mm thick aluminium casing. During use, both detectors were positioned with their long-axis parallel to the ground surface for greatest sensitivity (Fig. S1). The maximum count-rate of each detector was 30,000 counts per second (CPS), with a total energy range of 0–1.5 MeV across the unit's 4096 channels. Whilst both the detector and GPS receiver were mounted at the end of the length of tubing - the associated control electronics for the two units were located inside the operator's backpack. The operator walked throughout the entire area of the site, including walking over the surface of the stacked bags of contaminated topsoil. Data was recorded simultaneously, in real-time, onto micro SD-cards for subsequent data processing and interpretation.

Calibration of the units was crucial to ensure that measurements taken by each of the detectors were directly comparable and results accurate. Prior to fieldwork within a laboratory setting, both units were calibrated by positioning differing activity radiocesium sources at varying separations from each detector. The results of this calibration are presented in Fig. S2 - from this plot it is apparent that measurements from both units are directly comparable to one another. To calculate the conversion between the measured intensity in counts per unit time and air dose rate ($\mu Sv\ h^{-1}$), a single detector was placed alongside a RADEX (Moscow, Russia) dosemeter and exposed to a variety of radiocesium sources of differing activities at a range of distances. For each measurement, the counts from the detector were recorded with the dose measured and plotted in Fig. S3. The calculated linear relationship was subsequently used to convert the counts per second to air dose rate within the final map.

Whilst in the field, a further calibration was conducted to ensure that measurements from both of the gamma-ray spectrometers were directly comparable. To achieve this; the operator would walk along a predetermined path in one direction, before turning around and returning to the start point along the same route - exposing each of the detectors to the same radiation field. A comparison of the measurements obtained by each detector is shown in Fig. S4. Like the laboratory-based calibration, the results of this calibration reveal the high-degree of similarity between both detectors during the two test transects.

2.2. Unmanned aerial vehicle

After performing the radiation survey of the site using the backpack mounted system, an unmanned aerial vehicle (UAV) was used to capture an array of substantially overlapping images for a photogrammetry reconstruction of the site (Fig. 3 (b)) (section 2.3, below). The UAV used to capture the images was a lightweight system designed and constructed at the University of Bristol (UK), and consisted of a platform with an X4 configuration, powered by two lithium-polymer (LiPo) batteries. Carrying a 125 g digital camera, the system was capable of a total flight time of 30 min of typical operation on a single charge of its batteries. For flexibility and to reduce the overall cost of the platform to approximately £500, the UAV was constructed entirely out of commercially available parts with no specific machining of parts required.

For each flight, both take-off and landing were controlled by the operator using conventional hand-held remote controls. An initial system test was also performed at this point prior to undertaking the autonomous survey. Once airborne, the UAV conducted image acquisition of the site fully-autonomously via a series of pre-programmed GPS waypoints and altitudes - at a constant ground-equivalent velocity of 1.0 m s^{-1}.

2.3. Photogrammetry

Photogrammetry is a method of extracting geometric information from a series of overlapping 2D images of an area without the requirement for being in direct contact with its surface (Schenk, 2005). In applications relating to the remote sensing of the environment, this terrain reconstruction technique is a low-cost method with which to generate centimetre accurate digital surface models (DSMs); permitting the representation of any environment in three dimensions.

The camera used during this study was a Panasonic™ Lumix™ Tough Compact camera (model: DMC-FT30EB-D). This 16.1 megapixel system contained a 6.17 × 4.55 mm CCD sensor with both automatic image stabilisation and focusing - being able to acquire an image in continuous shooting mode up to eight times per

second. In order to obtain the images needed for the reconstruction, the lightweight unit was placed at nadir to the surveyed ground surface and images captured at a rate of one every second.

To achieve both the greatest spatial resolution possible whilst covering the largest area of the site possible, the survey was conducted at an altitude of 30 m above ground level (AGL) - the flight lines are represented by the individual camera locations in Fig. 5 (a). In total, 559 images were used for the reconstruction of the 3904 m^2 study area. The combination of the low flight altitude and the high number of source images results in an excellent degree of overlap between adjacent images (>90%) such that the majority of points within the site feature in greater than nine images used in the photogrammetric construction (Fig. 5 (a)). In typical photogrammetry reconstructions, a good level of overlap is considered to be approximately 80% between on-lapping (overlapping images in the direction of flight) images and 60–80% between side-lapping (overlapping images perpendicular to the direction of flight) images (Colomina and Molina, 2014).

The processing of the raw aerial images was conducted using AgiSoft Photoscan™. This commercial software package is widely used in environmental remote sensing due to its powerful capabilities in producing georeferenced DSM and orthophoto files in numerous coordinate systems; which can then be exported to geographic information systems (GIS) in order to be further manipulated or analysed with extra geospatial datasets (AgiSoft LLC, 2012). Photoscan™ is considered a largely autonomous process for creating 3D models, requiring only small inputs from the user in order to achieve a basic model. A generalised workflow for building a textured 3D model consists of aligning the images through pixel matching algorithms to form a 3D point-cloud. Following this, a surface mesh is interpolated between these points, which is then textured using colour information from the original source images used initially in the earlier alignment process (AgiSoft LLC, 2012).

In extracting the 3D points for the initial sparse point cloud, Photoscan uses a series of algorithms to first detect features on a series of reference images and then matches these to corresponding features within further images. On features with matches of good probability in a number of images, a least squares estimate is applied and any outliers removed from the matching. This process is similar to the Scale Invariant Feature Transform (SIFT) algorithm outlined by Lowe (2004), albeit with some alterations (Gonçalves and Henriques, 2015). With the conjugate sets of points between images identified and optimised, a network bundle adjustment algorithm is applied. This algorithm works towards providing the optimal solution of the 3D scene geometry using the estimated 3D scene coordinates, the camera poses and their calibrations (Triggs et al., 2000). The camera positions and parameters used within this step are retrieved from the EXIF data stored within the metadata of each JPEG image used in the alignment process.

Whilst the positions of the camera can be retrieved from the image metadata, a series of ground control points (GCPs) are needed to properly georeference the point cloud directly to a specific coordinate system and to a good degree of accuracy. Within the investigation area, five GCPs of known location were used - four located towards each corner of the site and one to the eastern edge. These locations were identified within the un-georeferenced point cloud and the bundle adjustment algorithm reapplied to optimise the point cloud into the WGS 1984 coordinate system.

Following the construction of the sparse point cloud, a multi-view stereo algorithm is used to create a dense point cloud (Gonçalves and Henriques, 2015). There are a number of reconstruction options to choose from during this step, referring to how much of the overall resolution is to be used from the input images. These range from 'Ultra High' (which uses the full initial image resolution) to 'Low'. The choice of appropriate resolution depends on the computing power available; for example, an investigation with an input of 500 images at a 12 megapixel resolution will require around 32 GB of available memory to fully reconstruct the dense point cloud at the 'Ultra High' reconstruction setting. In contrast, choosing the 'High' reconstruction setting for the same scenario requires an available memory of 8 GB (AgiSoft LLC, 2012). In light of this, the 'High' resolution (50% of the resolution of the source images) reconstruction setting was chosen to create the dense point cloud for the site, owing to the large number of images at a 16.1 megapixel resolution. The resultant DSM presented a resolution of 2.97 cm $pixel^{-1}$ with a total RMS error of 1.3 pixels. Following on from the selection of the 'High' resolution reconstruction mode, the orthophoto resolution is 1.49 cm $pixel^{-1}$. The final 3D surface model was created by overlaying the orthophoto onto the DSM surface within ArcGIS (section 2.4., below).

2.4. Model production

The construction of the 3D radiation map was conducted within ArcScene (the 3D visualisation front-end to the 3D Analyst extension of ESRI's ArcGIS package). The process combines the individual results of the radiation mapping survey and the photogrammetric reconstruction into a single interactive 3D radiation map. The radiation data, imported into ArcGIS as an XY point dataset (a series of individual points containing position, estimated altitude and radiation intensity data), was converted into a shapefile and interpolated to a continuous surface representation (a 32 bit floating point raster) using an inverse distance weighting (IDW) interpolation algorithm - pixels within the output raster file that have numerous measurements falling within their boundaries were instructed to use the average of these values. The resulting map was colour scaled according to a four-group classification, ranging from 0 to 5 $\mu Sv\ h^{-1}$, and contoured for clarity according to these break values. To complete the model, the colour-scaled radiation map was draped onto the 3D surface model at a constant elevation offset of 1 m above the DSM surface, which represents the approximate height above ground level that the measurements were recorded at throughout the survey.

3. Results and discussion

The results of the ground-based radiation mapping survey conducted over the site are shown in Fig. 4. As anticipated from a site that has seen extensive remediation and pre-treatment prior to transformation to a storage facility, the majority of the observed radiation anomaly exists within the boundaries of the stacked waste storage bags (area defined in Fig. 4). However, a distinct radiological signature exists away from the position of this confined waste material, downslope to the south.

Through the use of high spectral-resolution gamma-ray spectrometers, the nature of the radiation can be determined through the analysis of the gamma-rays emitted – a feature not available when using simpler and cheaper Geiger-Muller (GM) based units. The gamma-spectra obtained from three positions across the site (i, ii and iii) are shown in Fig. 4 (b–d) respectively. Apparent is the identical nature of each of these spectra; showing the characteristic peaks of the highly-volatile and high-yield fission product cesium. Each of the spectra (i, ii and iii) all show contributions from both the shorter-lived isotope ^{134}Cs (peaks at 569, 605 and 796 keV, half-life = 2.0652 years), which has subsequently decayed through several half-lives since its release into the environment, as well as the longer-lived ^{137}Cs (peak at 662 keV, half-life = 30.17 years) - which will present a radiological hazard for the foreseeable future.

As a direct result of the prevailing climate within this region of

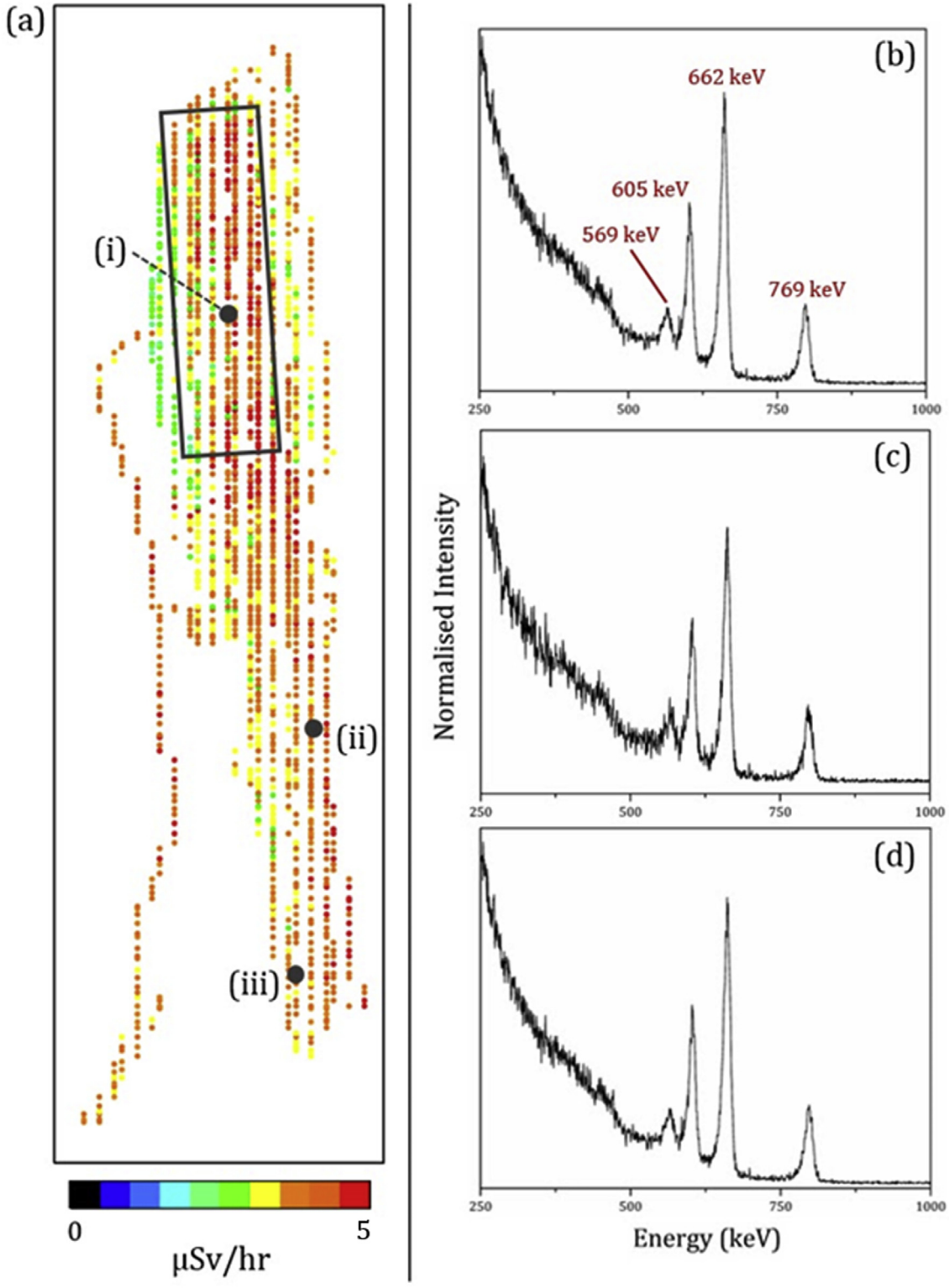

Fig. 4. Radiation map of the region (location of material shown) (a), with the gamma-ray spectrum obtained from the three positions shown (i, ii and iii as plots b, c and d respectively). The energies of each of the peaks are identified, resulting as the product the decay of ^{134}Cs (569, 605 and 796 keV) and ^{137}Cs (662 keV) respectively.

Japan (being characterised by typhoon conditions with extensive rainfall events) and the exposed nature of the waste material stored at these sites, there is the strong likelihood that material will be re-mobilised and transported from its point of origin - such movement has been shown to occur by a number of earlier works on sites across the affected Fukushima Prefecture (Evrard et al., 2013; Ueda et al., 2013; Yamashiki et al., 2014). This movement is seen to represent the transport of mineral and fine-scale particles in the environment onto which the radiocesium is strongly sorbed.

Whilst plans are currently being devised for the long-term

storage facility into which these considerable volumes of waste can be safely stored, it was envisaged that these small temporary facilities would provide suitable safe and secure storage of material whilst these final strategies are produced. Despite this, the escape of contamination is evident from this particular store; which had yet to be completed by covering the large 1 m^3 bags with an impermeable membrane to prevent against further water ingress and subsequent radioisotope-laden outflow.

The high-resolution modelling of the site, shown in Fig. 5 (b), illustrates a 3D snapshot of the distribution of the radiological material at the time of the field investigation (October 2016). In parallel to this investigation, a small number of radiometric measurements were recorded at a second site that had not yet been subjected to the pre-processing efforts applied to the modelled site. The results demonstrated that a suitable approximation for the initial intensity (before any pre-processing) for sites in this area range between approximately 3.2–3.6 μSv h^{-1}. Whilst no comparable value was recorded for the modelled site (as it had already undergone pre-processing at the time of the investigation), it is reasonable to assume that the remediated intensity levels would be reduced by this pre-processing.

Across the site, more than 7000 individual measurements were recorded by the dual detector system. The average intensity value was calculated to be 3.80 μSv h^{-1} for the site as a whole, whilst the average intensities for the areas both enclosed by the bale stack and outside this perimeter were calculated as 4.02 and 3.70 μSv h^{-1} respectively. Through visual inspection, there exist three main regions of interest within the site; all displaying elevated 'hotspot' levels of radiation intensity (herein 'hotspot' refers to regions of measured intensity exceeding 4 μSv h^{-1} (the mean intensity of the bale stack and indicated by the colour red in Fig. 5 (b)). As expected, the largest hotspot (i) is focussed directly within and immediately surrounding the bale stack, indicating that a large proportion of the radiological material is contained within this region. The geometry of this high intensity region and the bale stack correlate reasonably well, although localised variation in measured intensity is observed, where values drop to as low as 2.8 μSv h^{-1} in small pockets (blue within Fig. 5 (b)). There could be several possible

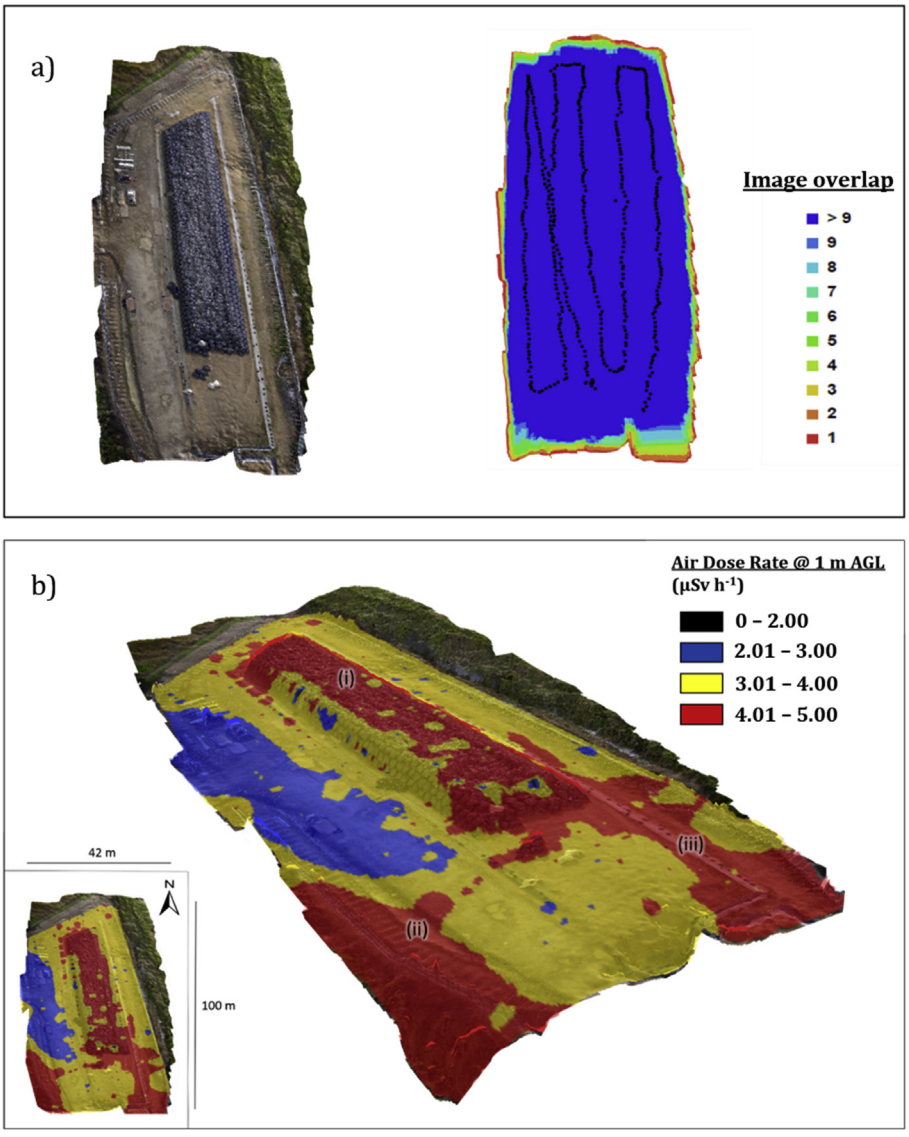

Fig. 5. a) 2-dimensional rendering of the study site (left) alongside camera locations (black dots) and the image overlap data for the site (right). b) 3-dimensional rendering of the study site. A coloured scaling depicting the measured radiation intensity is overlain onto the photogrammetry-derived data. (For interpretation of the references to colour in this figure legend, the reader is referred to the web version of this article.)

explanations for this observed pattern. For instance, the existence of natural variability in the distribution of radiological material in the initial contaminated topsoil. Alternatively, there could be some element of self-shielding occurring within the stack, which could introduce a directional component to the gamma-ray emission; reducing measured intensity within certain parts of the survey according to the source-detector geometry. This effect would possibly be further amplified by the directional sensitivity of the two SIGMA-50™ detector units, which can produce a disparity of up to 0.3 μSv h^{-1} between source-detector geometries focussed on its long axis and cross-sectional face (Fig. S1). The effects of this would be most prevalent when surveying alongside the long-axis borders of the bale stack, where most of this localised variation is observed.

The further two hotspot regions (ii) and (iii) suggest that the proposed containment of the material within the perimeter of the bales has been unsuccessful. These zones would represent a major concern for the authorities involved in constructing and maintaining this interim storage facility as they depict a migration of radiological material from the bale perimeter and into the environment. The hotspot at (ii) seemingly extends from the southern perimeter of the bale stack more than 30 m past the south-eastern limits of the modelled site. In contrast, (iii) seemingly extends around 15–20 m towards the south-western corner of the modelled site and past the limits of the investigated area. The direction and magnitude of the migration of the radiological material through this site is likely facilitated through the surface runoff processes: both hotspots appear to show downslope migration from the southern edge of the large bale stack, exhibiting erratic stream-like geometries, as illustrated by surface hydrological effects.

In order to visualise these effects on the hotspot regions, further work was conducted to determine the flow accumulation across the site. By using a representation of the local surface (DSM) and splitting this area into a raster grid, a flow accumulation dataset determines the amount of water accumulating within a cell by calculating the number of upslope cells that drain into the cell. The surface representation is usually a digital terrain model (DTM) or a digital elevation model (DEM), which the algorithms use to determine the magnitude of the flow accumulation based upon the topographic geometry of the area. Within the output dataset, cells with high values can be considered as areas of concentrated flow, which will help to identify the presence of stream flow regions within an area (Jenson and Domingue, 1988)

The output dataset from the hydrological modelling is shown overlain onto the radiation model in Fig. 6. From this, a few conclusions about the basic hydrology of the site can be drawn: Firstly, the bale stack sits on a slight topographic high relative to the outer fringes of the site, which is likely to be an intentional product of the pre-processing procedure; deliberately directing flow away from the bale stack towards the southern and eastern/western fringes of the site. Even without the aid from the flow accumulation data, it is evident from the model that water accumulates within the stream channel that runs parallel to the western boundary of the site, indicated by the standing water visible within the orthophoto. The accumulation data indicates a good fit with this, illustrated by the large flow accumulation zones draining into this channel (Fig. 6 (i)). The locations of the significant flow accumulation zones within this south-west corner are complementary to the location and morphology of the radiological hotspot and provides good evidence for the mechanism by which the radiological material is transported to this corner of the site. However, a problem with this summation arises when considering that this hotspot (Fig. 5 (b) (ii)) should therefore sit in this channel and likely take on its morphology - as this is where material is most likely deposited within the site. This could however, be explained by considering that transportation of radiological material is only likely to occur when the relative energy of the water flowing across the site is sufficiently large (i.e. following a heavy storm or typhoon). Hence, the shallow channel would likely overflow, allowing material to spread beyond the boundaries of the site. Alternatively, this observed distribution could be distorted by data obtained from outside of the remediated area of the ISF (beyond the perimeter fence), which was recorded at the very start of the survey into the site. If this area is indeed unremediated relative to the interior of the site, then it could be creating an erroneously high intensity region close to the perimeter of the site and hence, falsely represent the migration of material past the channel. To sufficiently conclude as to whether the observed distribution is true, further investigation - for example soil sampling and screening - is required.

Towards the eastern boundary of the site, the flow is less easily defined on inspection of the orthophoto alone. However, the flow accumulation overlay illustrates that the flow occurs most strongly due south from the south-eastern corner of the bale stack, with further minor accumulation occurring in an easterly direction towards the vegetated bank on the outside of the site's fence. Once more, the location and morphology of the hotspot (Fig. 5 (b) (iii)) in this region reflects the flow accumulation well, indicating that surface flow across the site is likely to be the main transportation mechanism defining the hotspot regions away from the bale stack.

Thus far, only radiometric signatures of above 4 μSv h^{-1} have been considered as representative of material transport from the bale stack. This consideration reflects the lack of confident knowledge of the radiometric intensity of the site after the pre-processing but before the emplacement of the bales. If the remediation of the site within the pre-processing step was largely successful in reducing measurable intensity levels, then the issue of material transport across the site could be considerably more worrying for the responding authorities. Regions of transported material in this case could possibly be represented by measurements exceeding approximately 3.0–3.4 μSv h^{-1} (depending on the success of the remediation efforts). This would mean that everything represented yellow or red on the model would be considered to be re-mobilised material. Without this confident knowledge however, the previous definition stands as the qualifying factor.

Although the results from the hydrology study and the hotspot locations can be considered complementary, there are limitations to consider when using this method to illustrate the observed migration of radiological material around this location. The use of a DSM to represent the land surface is the major issue. A DSM represents all the features of the sampled land (the ground surface, buildings and vehicles in this case) as part of the topographic land surface, creating a continuous mesh between all the points used within the reconstruction. This therefore represents the bale stack as a fully impermeable surface that water must flow over instead of infiltrating between (or through) the constituent bags in the stack. This implies the creation of erroneous artefacts of accumulation of flow in areas on and proximal to the bale stack, but is unlikely to affect accumulation results too much further afield from the stack boundaries, hence the findings discussed above remain valid. The alternative to this would be to use a digital terrain model (DTM), which would represent only the basic topography (no buildings, vehicles or bales). Whilst this would also not fully represent the site (as the bales would not be present) the two models would provide end-member hydrology datasets which could be used in tandem to improve the subsequent interpretation.

A further problem exists within the photogrammetric surface reconstruction, which experiences greater error towards the fringes of the surveyed area due to the reduced number of shared points between different photos (Fig. 5 (a)). This may be inserting poorly

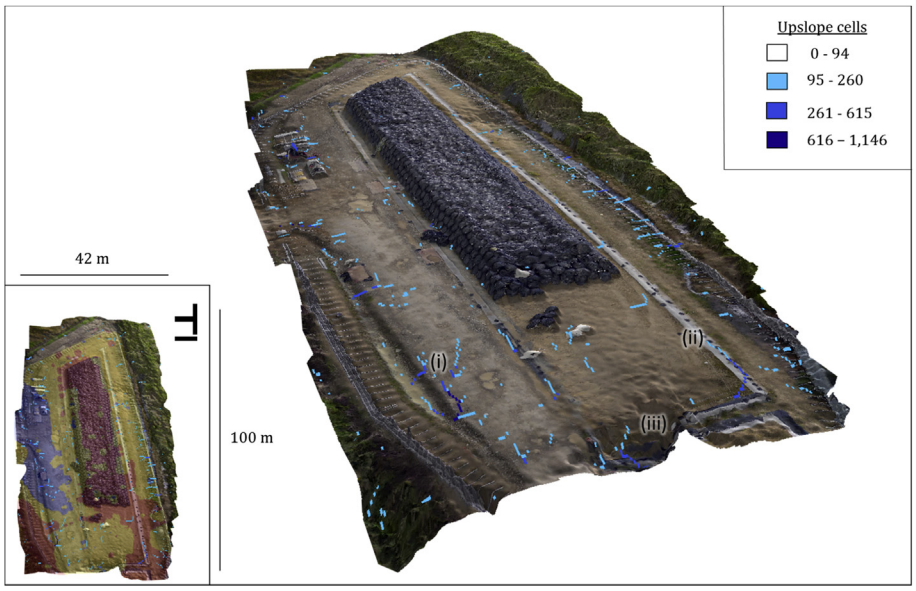

Fig. 6. 3-dimensional rendering of the study site with the flow accumulation dataset overlain onto the surface. Low level accumulation data (<94 upslope draining cells) has been removed to increase clarity.

reconstructed surfaces into the dataset - resulting in ridges and depressions in the model that do not exist within the surface of the site - which would propagate into the results from the flow accumulation study (i.e. Fig. 6 (iii)). Subsequently, this reduces the certainty in the conclusions for the regions very close to the exterior of the modelled site. For this study however, the regions of interest with respect to the radiation measurements do not fall in any low confidence zone (i.e. Fig. 6 (iii)). Future work to reduce these factors will include using 3D scanning LiDAR systems as a UAV payload, creating the possibility to produce both DSMs and DTMs with millimetre accuracy. This would allow for both end-member flow accumulation studies to be analysed to further constrain the transportation pathways across the site.

A final consideration of the limitations within this methodology is the contribution of GPS error throughout the site survey. The Adafruit™ GPS receiver presents an absolute position accuracy of approximately 2.5–3 m. Whilst this is a standard accuracy across the units available on the market, it presents the possibility that some of the intensity readings could be erroneously located within a 2.5 m radius of their actual position, which could have negative implications on the subsequent interpretation of the arising intensity map. However, the advantage of the dual GPS system (with a constant 2.3 m separation between each unit) within this investigation is that erroneously located measurements can be identified before the interpolation of the data points within the post-processing stage, allowing for greater confidence within the accuracy of the positioning of this system. In the future, moving to a differential GPS system may be prudent; these systems contain two individual receivers – one static (ground station), the other based on the moving device - that communicate with each other as well as the space segment of the GPS network. By tracking the position of the moving receiver relative to the orbiting satellites and the static ground station, position accuracies on the order of centimetres can be achieved (Mueller et al., 1992; Jiang and Sun, 2017).

4. Conclusions and future work

This work has successfully shown (i) the application of combined ground-based radiation mapping alongside airborne photogrammetry for providing a highly-visual representation of a contaminated site, and (ii), that the movement of radiological material is occurring from this, and potentially other, waste storage facilities within Fukushima Prefecture.

In contrast to “traditional” radiological surveys whereby the results obtained are expressed simply as a scaled overlay onto a background map, the combined application of an initial foot-based survey and a later aerial survey has shown to be an enormously powerful method with which to visualise contamination over a three-dimensional surface. Applying fluidic processes to the model has also permitted the study of resultant species transport.

The site is similar to hundreds of others located around the Fukushima area, with many other sites however being considerably larger in their spatial extent. Whilst measures are put in place to guard against contaminant outflow post-completion of the project (by installation of an impermeable barrier) as is evidenced here, considerable contaminant transport has already occurred prior to this action occurring. As a result, further studies of other such sites are duly required in order to establish how widespread these findings are and if measures need to be enacted early on during the construction of these facilities in order to prevent against contaminant outpouring.

The entire ground-based radiological survey of the approximately 40 × 100 m site was undertaken in a total of 20 min - walking over the uneven morphology of the site. The subsequent aerial photogrammetry survey was also performed in under a total of 20 min – combined representing an extremely rapid method of site characterisation. Using a low-cost digital camera reduces the total operating cost of the platform considerably when compared with other digital surface reconstruction techniques such as 3D-scanning LiDAR, where the cost of such units can typically exceed $50,000. One drawback, however, in the use of airborne photogrammetry is the time and computational performance required to post-process the data obtained from each survey flight.

Whilst the use of the novel dual-detector system offers the capability for increased repeatability and comparability between surveys conducted by different operators, it does not represent the optimal solution for maximum repeatability between surveys across the temporal domain. This is because the system is

inherently affected by the inability of any human operator to walk exactly the same survey lines, at exactly the same speed. These factors become even more of a problem when using different operators to repeat the same surveys, as is the case within the radiological monitoring procedure currently being used within the ISF sites. These problems could be overcome by incorporating integrated UAV systems within the standard radiological monitoring protocol. These systems are capable of flying pre-programmed waypoint routes, which can be stored and reused whenever required, creating the capability for fully repeatable surveys irrespective of the operator (as long as the pre-programmed flight parameters remain constant). It would seem therefore, that for the application of radiological monitoring over the temporal domain, UAVs represent a valuable and under-utilised resource.

Current work is continuing to evolve the airborne system still further. This work will see the UAV perform simultaneous airborne radiation mapping alongside digital image capturing. Post-acquisition, the application of digital ray-tracing simulations to back-trace the detected radiation to its emission source will be applied to the data obtained. Further fieldwork within the Fukushima Prefecture is planned for June 2017, including a re-visit to the modelled ISF within this investigation. A key aspect of this further work will be to determine the viability of UAV-based radiation surveying to repeatedly map waste storage sites, producing exactly comparable data between surveys of the same site taken but at different times. Such a capability would prove invaluable for improving the quality of the existing monitoring programme in the Fukushima prefecture.

Acknowledgements

The authors wish to thank the Daiwa Anglo-Japanese Foundation (Ref: 6102/12029) for kindly providing funding to enable this work within Japan. The financial support from the UK NNL (NNL/UA/037), EPSRC (EP/N509619/1) and Perry Noble Scholarship are also acknowledged for funding the studentships of DC and PGM respectively. Support from local officials and members of the public within Fukushima Prefecture is greatly appreciated for facilitating access to such study sites. NTS is supported by a Royal Society Industry Fellowship and the NNL IR&D Programme.

Appendix A. Supplementary data

Supplementary data related to this article can be found at https://doi.org/10.1016/j.envpol.2017.10.098.

References

Adafruit, n.d. Adafruit Ultimate GPS Breakout - 66 channel w/10 Hz updates - Version 3. URL https://www.adafruit.com/product/746 (accessed 16.08.17).
AgiSoft LLC, 2012. AgiSoft PhotoScan User Manual - Professional Edition, Version 0.9.0.
Buchanan, E., Cresswell, A.J., Seitz, B., Sanderson, D.C.W., 2016. Operator related attenuation effects in radiometric surveys. Radiat. Meas. 86, 24–31. https://doi.org/10.1016/j.radmeas.2015.12.029.
Colomina, I., Molina, P., 2014. Unmanned aerial systems for photogrammetry and remote sensing: a review. ISPRS J. Photogramm. Remote Sens. https://doi.org/10.1016/j.isprsjprs.2014.02.013.
Connor, D., Martin, P.G., Scott, T.B., 2016. Airborne radiation mapping: overview and application of current and future aerial systems. Int. J. Remote Sens. 37 (24), 5953–5987. https://doi.org/10.1080/01431161.2016.1252474.
Evrard, O., Chartin, C., Onda, Y., Patin, J., Lepage, H., Lefèvre, I., Ayrault, S., Ottlé, C., Bonté, P., 2013. Evolution of radioactive dose rates in fresh sediment deposits along coastal rivers draining Fukushima contamination plume. Sci. Rep. 3, 3079. https://doi.org/10.1038/srep03079.
Gonçalves, J.A., Henriques, R., 2015. UAV photogrammetry for topographic monitoring of coastal areas. ISPRS J. Photogramm. Remote Sens. 104, 101–111. https://doi.org/10.1016/j.isprsjprs.2015.02.009.
IAEA, 2008. The International Nuclear and Radiological Event Scale User's Manual. International Atomic Energy Agency, Vienna, Austria.
JAEA, 2017. Airborne Monitoring in the Distribution Survey of Radioactive Substances (FY 2011-FY 2016 The Ministry of Education, Culture, Sports, Science and Technology, the U.S. Department of Energy, and the Secretariat of the Nuclear Regulation Authority). Available at: emdb.jaea.go.jp/emdb/en/portals/b136/. . (Accessed 22 February 2017).
Japan Meteorological Agency, n.d. Monthly total of precipitation (mm) - Japan Meteorological Agency [WWW Document]. URL http://www.data.jma.go.jp/obd/stats/etrn/view/monthly_s3_en.php?block_no=47401&view=13 (accessed 1.14.16).
Japanese Ministry of the Environment, 2012. Management of off-site Waste Contaminated with Radioactive Materials Due to the Accident at Fukushima Nuclear Power Stations. Tokyo.
Jenson, S.K., Domingue, J.O., 1988. Extracting topographic structure from digital elevation data for geographic information system analysis. Photogramm. Eng. Remote Sens. 54, 1593–1600, 0099-1112/88/5411-1593$02.25/0.
Jiang, H. and Sun, X. 2017. A Camera Calibration Method Based on Differential GPS System for Large Field Measurement, in. Springer, Cham. 508–519. 10.1007/978-3-319-65292-4_44.
Jones, H.E., Cunningham, J.R., 1983, 4th Edition. In: Physics of Radiology, fourth ed. Thomas Publishing, Springfield, Illinois, USA.
MacFarlane, J.W., Payton, O.D., Keatley a, C., et al., 2014. Lightweight aerial vehicles for monitoring, assessment and mapping of radiation anomalies. J. Environ. Radioact. 136, 127–130. https://doi.org/10.1016/j.jenvrad.2014.05.008.
Martin, P.G., Payton, O.D., Fardoulis, J.S., Richards, D.A., Scott, T.B., 2015. The use of unmanned aerial systems for the mapping of legacy uranium mines. J. Environ. Radioact. 143, 135–140. https://doi.org/10.1016/j.jenvrad.2015.02.004.
Martin, P.G., Payton, O.D., Yamashiki, Y., Richards, D.A., Scott, T.B., 2016a. High-resolution radiation mapping to investigate FDNPP derived contaminant migration. J. Environ. Radioact. 164, 26–35. https://doi.org/10.1016/j.jenvrad.2016.06.025.
Martin, P.G., Payton, O.D., Fardoulis, J.S., Richards, D.A., Yamashiki, Y., Scott, T.B., 2016b. Low altitude unmanned aerial vehicle for characterising remediation effectiveness following the FDNPP accident. J. Environ. Radioact. 151, 58–63. https://doi.org/10.1016/j.jenvrad.2015.09.007.
Martin, P.G., Kwong, S., et al., 2016c. 3D unmanned aerial vehicle radiation mapping for assessing contaminant distribution and mobility. Int. J. Appl. Earth Observation Geoinformation 52, 12–19.
Mueller, K., Loomis, P., Kalafus, R.S.L., 1992. Networked Differential GPS System. Available at: https://www.google.com/patents/US5323322 (Accessed: 16 August 2017).
Nagao, S., Kanamori, M., Ochiai, S., 2013. Export of 134 Cs and 137 Cs in the Fukushima river systems at heavy rains by typhoon roke in September 2011. Biogeosciences. https://doi.org/10.5194/bg-10-6215-2013.
Schenk, T., 2005. Introduction to Photogrammetry. Dep. Civ. Environ. Eng. Geod. Sci. Ohio State Univ., pp. 79–95
Triggs, B., McLauchlan, P.F., Hartley, R.I., Fitzgibbon, A.W., 2000. Bundle adjustment — a modern synthesis. Vis. Algorithms Theory Pract. 1883, 153–177. https://doi.org/10.1007/3-540-44480-7_21.
Ueda, S., Hasegawa, H., Kakiuchi, H., Akata, N., Ohtsuka, Y., Hisamatsu, S., 2013. Fluvial discharges of radiocaesium from watersheds contaminated by the Fukushima Dai-ichi nuclear power plant accident. Jpn. J. Environ. Radioact. 118, 96–104. https://doi.org/10.1016/j.jenvrad.2012.11.009.
Yamaguchi, N., Eguchi, S., Fujiwara, H., Hayashi, K., Tsukada, H., 2012. Radiocesium and radioiodine in soil particles agitated by agricultural practices: field observation after the Fukushima nuclear accident. Sci. Total Environ. 425, 128–134. https://doi.org/10.1016/j.scitotenv.2012.02.037.
Yamashiki, Y., Onda, Y., Smith, H.G., Blake, W.H., Wakahara, T., Igarashi, Y., Matsuura, Y., Yoshimura, K., 2014. Initial flux of sediment-associated radiocesium to the ocean from the largest river impacted by Fukushima Daiichi Nuclear Power Plant. Sci. Rep. 4, 3714. https://doi.org/10.1038/srep03714.
Yasutaka, T., Naito, W., 2015. Assessing cost and effectiveness of radiation decontamination in Fukushima Prefecture. Jpn. J. Environ. Radioact. https://doi.org/10.1016/j.jenvrad.2015.05.012.